International Conference on Mathematics, Computational Methods & Reactor Physics (M&C 2009)
Saratoga Springs, New York, May 3-7, 2009, on CD-ROM, American Nuclear Society, LaGrange Park, IL (2009)

ANALYTICAL RECONSTRUCTION SCHEMES FOR COARSE-MESH SPECTRAL NODAL SOLUTION OF SLAB-GEOMETRY S_N TRANSPORT PROBLEMS

Ricardo C. Barros, Hermes Alves Filho, Gustavo M. Platt, Francisco Bruno S. Oliveira* and Damiano S. Militão

Programa de Pós-graduação em Modelagem Computacional, Instituto Politécnico (IPRJ/UERJ)
Rua Alberto Rangel s/n, 28630-050 Nova Friburgo, RJ, Brazil
rcbarros@pq.cnpq.br, halves@iprj.uerj.br, gmplatt@iprj.uerj.br, fbrunoso@uol.com.br, mestredam@yahoo.com.br

ABSTRACT

Coarse-mesh numerical methods are very efficient in the sense that they generate accurate results in short computational time, as the number of floating point operations generally decrease, as a result of the reduced number of mesh points. On the other hand, they generate numerical solutions that do not give detailed information on the problem solution profile, as the grid points can be located considerably away from each other. In this paper we describe two analytical reconstruction schemes for the coarse-mesh solution generated by the spectral nodal method for neutral particle discrete ordinates (S_N) transport model in slab geometry. The first scheme we describe is based on the analytical reconstruction of the coarse-mesh solution within each discretization cell of the spatial grid set up on the slab. The second scheme is based on the angular reconstruction of the discrete ordinates solution between two contiguous ordinates of the angular quadrature set used in the S_N model. Numerical results are given so we can illustrate the accuracy of the two reconstruction schemes, as described in this paper.

Key Words: neutral particle transport, discrete ordinates, spectral nodal methods, spatial and angular reconstruction schemes

1. INTRODUCTION

A practical limitation of coarse-mesh methods is that they do not generate a detailed profile of the solution of the problem. One alternative way to go around this drawback is to use fine-mesh numerical methods, or proceed to reconstructing the coarse-mesh numerical solution.

The spectral nodal methods [1-4] are widely regarded as forming an accurate class of coarse-mesh methods for S_N problems in rectangular geometry. For slab-geometry S_N fixed source problems, the spectral nodal method, that we refer to as the spectral Green's function (SGF) nodal method generates numerical values for the cell-edge and cell-average angular fluxes in the N discrete angular directions that exactly agree with those of the analytical solution of the S_N equations, regardless of the definition of the spatial grid and apart from computational finite arithmetic considerations [1].

In this paper we describe two analytical reconstruction schemes for the coarse-mesh numerical solution generated by the SGF method for fixed-source one-speed azimuthally symmetric S_N neutron transport problems in slab geometry with linearly anisotropic scattering. That is, the spatial reconstruction scheme expresses the S_N solution in each

* current address: Universidade Estadual de Santa Cruz, DCET, Rodovia Ihéus/Itabuna, Km 16, 45662-000 Ilhéus, BA, Brazil.

spatial cell as a linear combination of the elementary solutions, that we determine by spectral analysis [1], and assigns boundary conditions at cell edges, that are given by the converged SGF results to obtain a system of N linear algebraic equations in N unknown expansion coefficients, which then yield the exact S_N solution at each point in the cell. Moreover, the angular reconstruction scheme yields approximate angular flux at any angular direction $-1 \le \mu \le 1$, except $\mu = 0$, where $\mu = \cos\theta$, with θ being defined as the polar angle; hence not only at the discrete ordinates directions ($\mu_n, n = 1:N$). To achieve this goal, we substitute the local solution within each cell of the spatial grid, as we determine by the spatial reconstruction scheme, into the integral source terms of the analytical first-order form of neutron transport equation in slab geometry with linearly anisotropic scattering and solve the resulting approximate differential equation analytically.

At this point we outline the content of the remainder of this paper: in the next section we describe the spatial and the angular reconstruction schemes of the SGF S_N coarse-mesh solution. In section 3 we present numerical results to a multilayer fixed source S_N problem in slab geometry, and we conclude with a brief discussion in section 4.

2. THE SPATIAL AND THE ANGULAR RECONSTRUCTION SCHEMES OF THE SGF S_N COARSE-MESH NUMERICAL SOLUTION

2.1. The Spatial Reconstruction Scheme

Let us consider Fig.1 which represents a spatial discretization cell, also termed node Λ_j with the incoming angular fluxes as generated by the SGF nodal method, which is free from spatial truncation errors [1]. At this point we remark that the cell-edges have been defined as $x_{j-1/2} = 0$ and $x_{j+1/2} = h_j$, j=1:J, to avoid finite arithmetic overflow in coarse spatial grids as we need to evaluate exponential functions with positive exponents, as we describe next.

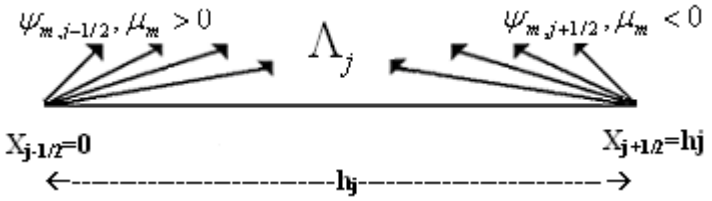

Figure 1. Spatial node Λ_j of width h_j with the incident angular fluxes as generated by the SGF nodal method.

To describe the spectral analysis we perform to the S_N equations inside node Λ_j in order to obtain the SGF nodal method, it is convenient to write the one-speed slab-geometry S_N equations in Λ_j with linearly anisotropic scattering in the following operator notation:

$$L_N\left[\psi_m(x)\right] \equiv \left[\frac{\mu_m}{\sigma_{Tj}}\frac{d}{dx} + 1 - \frac{c_{0j}}{2}\sum_{n=1}^{N}(\cdot)\omega_n - \frac{3c_{1j}}{2}\mu_m\sum_{n=1}^{N}\mu_n(\cdot)\omega_n\right]\psi_m(x) = \frac{Q_j}{2\sigma_{Tj}}, \qquad x \in \Lambda_j \tag{1}$$

where

$\psi_m(x)$: angular flux of particles traveling in the discrete ordinates direction μ_m ;
ω_m : angular weight for direction μ_m ;
σ_{Tj} : total macroscopic cross section;
Q_j : uniform and isotropic interior source;
$c_{kj} = \sigma_{Skj}/\sigma_{Tj}$, k = 0 , 1.

Here σ_{S0j} and σ_{S1j} are the zero'th and first-order components of the differential scattering cross section respectively. The general solution set K of Eq. (1) can be written as

$$K = \left\{ \psi_m^p(x) \right\} + kernel(L_N), \qquad x \in \Lambda_j \tag{2}$$

where

$$kernel(L_N) = span\left\{ \psi_m^h(x) \,|\, L_N[\psi_m^h(x)] = 0 \right\}, \qquad x \in \Lambda_j \tag{3}$$

and a particular solution appears as

$$\psi_m^p(x) = \frac{Q_j}{2\sigma_{Tj}(1 - c_{0j})} . \tag{4}$$

Now, to determine kernel(L_N), it is sufficient to find a basis for it. Therefore, we consider the *ansatz*

$$\psi_m^h(x) = a_m(\vartheta) e^{-\sigma_{Tj} x/\vartheta} , \tag{5}$$

where the constants $a_m(\vartheta)$ are normalized by

$$\sum_{n=1}^{N} a_n(\vartheta)\omega_n = 1 . \tag{6}$$

Substituting Eq. (5) into Eq. (3) and using Eq. (6), we obtain after some algebra

$$a_m(\vartheta) = \frac{c_{0j}\vartheta + 3\vartheta^2 c_{1j}(1 - c_{0j})\mu_m}{2(\vartheta - \mu_m)} . \tag{7}$$

Furthermore, we substitute Eq. (7) into Eq. (6) to obtain the S_N dispersion relation

$$\frac{1}{2}\sum_{n=1}^{N} \frac{c_{0j}\vartheta + 3\vartheta^2 c_{1j}(1 - c_{0j})\mu_n}{(\vartheta - \mu_n)}\omega_n = 1 , \tag{8}$$

whose N simple real roots ϑ_k are located symmetrically about the origin for any c_{oj} and c_{1j} satisfying $0 \leq c_{0j}, c_{1j} < 1$. Combining Eqs. (5) and (7), we obtain

$$\psi_{m,k}^h(x) = \left[\frac{c_{0j}\vartheta_k + 3\vartheta_k^2 c_{1j}(1 - c_{0j})\mu_m}{2(\vartheta_k - \mu_m)}\right] e^{-\sigma_{Tj} x/\vartheta_k} , \; m = 1{:}N , \; k = 1{:}N , \; x \in \Lambda_j . \tag{9}$$

Therefore, for $x \in \Lambda_j$ we have a linearly independent set of N elementary functions that forms a basis for *kernel*(L_N). From Eqs. (2) and (4) we write the general solution set

$$K = \left\{ \psi_m(x) \mid \psi_m(x) = \frac{Q_j}{2\sigma_{Tj}(1-c_{0j})} + \sum_{k=1}^{N} \alpha_k \psi^h_{m,k}(x) \ , \ \alpha_k \in \Re \right\} \ , \tag{10}$$

where $\psi^h_{m,k}(x)$, $x \in \Lambda_j$, is given by Eq. (9). Equation (10) is an expression for the general solution set of the S_N equations in Λ_j. The SGF nodal method is a convergent numerical method for the S_N problem represented in Eq. (1) such that

- ✓ the solution set K is preserved automatically;
- ✓ the solution is continuous across each node edge of the spatial grid set up on the slab;
- ✓ the solution satisfies the boundary conditions on the outer boundaries of the slab.

Therefore, the numerical solution generated by the SGF method has no spatial truncation error. A more detailed description of the SGF nodal method can be found in Ref. [1].

To proceed further with the spatial reconstruction scheme, we first set $x_{j-1/2} = 0$ and then $x_{j+1/2} = h_j$ in expression (10) of the analytical general solution in Λ_j. As the values of $\psi_{m,j-1/2}, \mu_m > 0$ and $\psi_{m,j+1/2}, \mu_m < 0$ have been determined previously by the SGF nodal method, we can solve the system

$$\mathbf{A}\boldsymbol{\alpha} = \mathbf{b} \tag{11}$$

of N algebraic linear equations for the N unknown $\alpha_\ell, \ell = 1:N$. In Eq. (11) we have defined the entries of the $N \times N$ square matrix **A** as

$$A_{i,k} = \begin{cases} \dfrac{c_{0j}\vartheta_k + 3\vartheta_k^2 \ c_{1j}(1-c_{0j})\mu_i}{\vartheta_k - \mu_i}, k = 1:N, i = 1:N/2 \ (\mu_i > 0) \\ \dfrac{c_{0j}\vartheta_k + 3\vartheta_k^2 \ c_{1j}(1-c_{0j})\mu_i}{\vartheta_k - \mu_i} \exp(-\sigma_{Tj} h_j / \vartheta_k), k = 1:N, i = (N/2)+1:N \ (\mu_i < 0). \end{cases} \tag{12}$$

In addition, the components of the column vector **b** are defined as

$$b_n = \begin{cases} \psi_n(0) - \dfrac{Q_j}{2\sigma_{Tj}(1-c_{0j})}, n = 1:N/2 \\ \psi_n(h_j) - \dfrac{Q_j}{2\sigma_{Tj}(1-c_{0j})}, n = (N/2)+1:N. \end{cases} \tag{13}$$

To conclude the spatial reconstruction scheme, we solve system (11) for the constants $\alpha_\ell, \ell = 1:N$, substitute them back into the local general solution, so we can evaluate the angular flux in the discrete direction at any point $x \in \Lambda_j$. At this point we remark that all spatial cells of the same material zone that have the same width will have identical matrix **A** *cf.* Eq. (12). However, the constants α_ℓ may be different as the components of the column vectors **b** may be also different, as they depend on the coarse-mesh solution generated by the SGF nodal method in accordance with Eq. (13).

2.2. The Angular Reconstruction Scheme

Once we have described an algorithm to perform spatial reconstruction within each spatial node Λ_j, j=1:J, of the coarse-mesh discretization grid, we proceed to describing an algorithm to perform angular reconstructions for any possible value (except $\mu = 0$) of the direction-of-motion variable $\mu\ (-1 \le \mu \le 1)$ and not only in the discrete ordinates directions as generated by the S_N SGF code. Therefore, let us use the standard definitions [5] of neutron scalar flux

$$\phi(x) = \frac{1}{2}\int_{-1}^{+1} \psi(x,\mu')\ d\mu' \cdot \tag{14a}$$

and neutron total current

$$J(x) = \frac{1}{2}\int_{-1}^{+1} \mu'\psi(x,\mu')\ d\mu' \cdot \tag{14b}$$

Therefore, using the expression for the local general solution in the S_N approximations to Eqs. (14a-b), we obtain

$$\phi(x) \cong \frac{1}{2}\sum_{\ell=1}^{N} \alpha_\ell\ e^{-\sigma_{Tj}\,x/\vartheta_\ell} + \frac{Q_j}{2\sigma_{Tj}(1-c_{0j})} \tag{15a}$$

and

$$J(x) \cong \frac{(1-c_{0j})}{2}\sum_{\ell=1}^{N} \alpha_\ell \vartheta_\ell e^{-\sigma_{Tj}x/\vartheta_\ell} \quad , \tag{15b}$$

where we have used the normalization condition (6) and the well known angular quadrature properties. Now we substitute the approximations given in Eqs. (15a-b) into the analytical neutron transport equation and solve the resulting equation analytically for the neutron angular flux $\psi(x,\mu),\ x \in \Lambda_j$. For $0 < \mu \le 1$, the result is

$$\psi(x,\mu) = \psi(0,\mu)\exp(\frac{-\sigma_{Tj}\,x}{\mu}) + \frac{c_{0j}}{2}\sum_{\ell=1}^{N}\frac{\alpha_\ell\vartheta_\ell}{(\mu-\vartheta_\ell)}[\exp(\frac{-\sigma_{Tj}\,x}{\mu}) - \exp(\frac{-\sigma_{Tj}\,x}{\vartheta_\ell})] +$$

$$\frac{3\,c_{1j}}{2}\sum_{\ell=1}^{N}\frac{\alpha_\ell(\vartheta_\ell)^2}{(\mu-\vartheta_\ell)}[\exp(\frac{-\sigma_{Tj}\,x}{\mu}) - \exp(\frac{-\sigma_{Tj}\,x}{\vartheta_\ell})] + \frac{Q_j}{2\sigma_{aj}}[1 - \exp(\frac{-\sigma_{Tj}\,x}{\mu})] \quad , \tag{16}$$

$$x \in \Lambda_j \quad .$$

Here x = 0 is the left-hand side edge of node Λ_j and x = h_j is the right-hand side edge of node Λ_j, i.e., $0 \le x \le h_j$. Furthermore, for $-1 \le \mu < 0$, we obtain the result

$$\psi(x,\mu) = \psi(h_j,\mu)\exp\left(\frac{-\sigma_{Tj}(h_j - x)}{|\mu|}\right) +$$

$$\frac{c_{0j}}{2}\sum_{\ell=1}^{N}\frac{\alpha_\ell \vartheta_\ell}{(\vartheta_\ell + |\mu|)}\left[\exp\left(\frac{-\sigma_{Tj}\,x}{\vartheta_\ell}\right) - \exp\left(\frac{-\sigma_{Tj}(h_j - x)}{|\mu|}\right)\exp\left(\frac{-\sigma_{Tj}\,h_j}{\vartheta_\ell}\right)\right] + \tag{17}$$

$$\frac{3c_{1j}(1-c_{0j})}{2}\sum_{\ell=1}^{N}\frac{\alpha_\ell(\vartheta_\ell)^2}{(\vartheta_\ell + |\mu|)}\left[\exp\left(\frac{-\sigma_{Tj}\,x}{\vartheta_\ell}\right) - \exp\left(\frac{-\sigma_{Tj}(h_j - x)}{|\mu|}\right)\exp\left(\frac{-\sigma_{Tj}\,h_j}{\vartheta_\ell}\right)\right] +$$

$$\frac{Q_j}{2\sigma_{aj}}\left[1 - \exp\left(\frac{-\sigma_{Tj}(h_j - x)}{|\mu|}\right)\right], \quad x \in \Lambda_j \quad .$$

Equations (16) and (17) are the analytical solutions of the approximate neutron transport equation for all direction-of-motion variables $-1 \le \mu \le 1$, $\mu \neq 0$, wherein we have considered the S_N approximations for the scalar flux and total current given by Eqs. (15a-b). We remark that the N values of α_ℓ are determined by solving the linear system (11) with definitions (12) and (13), as described for the spatial reconstruction scheme. Moreover, we see in Eqs. (16) and (17) that the present angular reconstruction scheme is not valid for the particular case of $\mu = 0$.

3. NUMERICAL RESULTS

We consider a heterogeneous model problem that consists of a four-layer slab of thickness L = 20 cm, represented in Fig.2. The boundary conditions and source distribution are shown in Fig.2 and the cross sections for the four material zones are listed in Table I. To solve this test problem, we used the S_{128} Gauss-Legendre quadrature set, with a convergence criterion requiring the discrete maximum norm of the relative deviation between two iterates to be less than or equal to 10^{-7}.

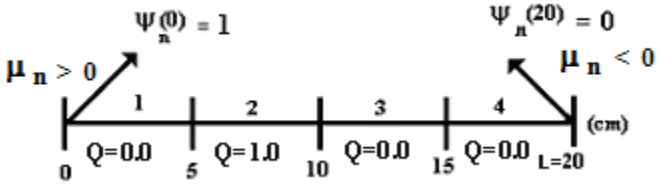

Figure 2. Model Problem

Table II shows the neutron fluxes in the angular directions μ_4 and μ_{120} of the conventional Gauss-Legendre S_{128} angular quadrature set at several positions on the slab represented in Fig.2. The fourth column of Table II displays the numerical results generated by the present spatial reconstruction scheme, wherein the incident cell boundary fluxes for the calculation of each set of constants were generated by the SGF code on a spatial grid composed of one cell per region. Furthermore, the fifth and the sixth columns show the angular fluxes as generated by the present angular reconstruction scheme, *cf*. Eq. (16) for $\mu_4 > 0$ and *cf*. Eq. (17) for $\mu_{120} < 0$. As we see, all relative deviations with respect to the SGF results displayed in the seventh column are no greater than 0.000122 % since the round off errors yielded very small discrepancies in some numerical results of this model problem.

Table I. Cross Sections for the Material Zones

Material Zone	σ_T	σ_{S0}	σ_{S1}
1	1.0	0.97	0.83
2	1.0	0.99	0.80
3	1.0	0.98	0.82
4	1.0	0.90	0.70

Table II. Neutron angular fluxes for the test problem

x (cm)	Angular direction (μ)[f]	$\psi_m(x)$ (SGF[c])	$\psi_m(x)$ (spatial reconstruction scheme)	$\psi(x,\mu)$ *cf.* Eq. (16)	$\psi(x,\mu)$ *cf.* Eq. (17)	δ [e] (%)
0[a]	μ_4	1.0	1.0	1.0		0.000000
	μ_{120}	4.3073202E+00[d]	4.3073174E+00		4.3073174E+00	0.000065
2[b]	μ_4	2.7521740E+00	2.7521749E+00	2.7521749E+00		0.000033
	μ_{120}	5.5685907E+00	5.5685873E+00		5.5685873E+00	0.000061
5[a]	μ_4	4.2360588E+00	4.2360588E+00	4.2360588E+00		0.000000
	μ_{120}	7.4049029E+00	7.4049029E+00		7.4049029E+00	0.000000
7[b]	μ_4	6.1427048E+00	6.1427017E+00	6.1427017E+00		0.000050
	μ_{120}	5.7090381E+00	5.7090376E+00		5.7090376E+00	0.000009
10[a]	μ_4	5.5984253E+00	5.5984253E+00	5.5984253E+00		0.000000
	μ_{120}	1.6628689E+00	1.6628684E+00		1.6628684E+00	0.000030
13[b]	μ_4	3.2391689E+00	3.2391701E+00	3.2391701E+00		0.000037
	μ_{120}	7.0834386E-01	7.0834389E-01		7.0834389E-01	0.000004
15[a]	μ_4	2.3398091E+00	2.3398091E+00	2.3398091E+00		0.000000
	μ_{120}	2.8351556E-01	2.8351551E-01		2.8351551E-01	0.000018
17[b]	μ_4	1.1465801E+00	1.1465815E+00	1.1465815E+00		0.000122
	μ_{120}	9.6857836E-02	9.6857660E-02		9.6857660E-02	0.000000
20[a]	μ_4	3.8153887E-01	3.8154201E-01	0.3815420E-01		0.000082
	μ_{120}	0.0	0.0		0.0	0.000000

[a] Numerical results generated by the SGF method [1] on a coarse spatial grid composed of one cell per region.
[b] Numerical results generated by the SGF method [1] on a spatial grid composed of five cells per region.
[c] SGF computer code.
[d] Read as 4.3073202.
[e] Relative deviation.
[f] μ_4 = 8.5463641E-02 and μ_{120} = - 9.7719849E-01 of the Gauss-Legendre S_{128}.

Now we perform a numerical experiment consisting of using a lower order Gauss-Legendre quadrature set, such as the S_8, to evaluate the neutron flux at x = 12 cm in the directions μ_1 = 0.339981043584856 and μ_4 = -0.861136311594053 that do not belong to the S_8 set, but rather to the S_4 Gauss-Legendre quadrature set. Therefore, we apply the present angular reconstruction algorithm:

(i) set up a coarse spatial grid on the slab represented in Fig. 2, composed of one cell per region;
(ii) run the SGF code using the S_8 Gauss-Legendre quadrature set and the material parameters listed in Table I;
(iii) use the converged angular fluxes entering region number 3 to evaluate the set of eight constants α_ℓ by solving system (11) with definitions (12) and (13);
(iv) use Eq. (16) with x = 2 cm (not 12 cm) and $\mu = \mu_1 = 0.339981043584856$ of the S_4 angular quadrature set together with the eight values of α_ℓ as determined in the previous step. The result is $\psi(12, \mu_1) =$ 4.4469161;
(v) proceed similarly for the case of $\mu = \mu_4 =$ -0.861136311594053 by using Eq. (17). The result is $\psi(12, \mu_4) =$ 1.2674364.

In order to check the results in this numerical experiment, we ran the SGF code using the Gauss-Legendre S_4 angular quadrature set on a finer spatial grid composed of five spatial cells per region. The angular fluxes at x = 12 cm in directions μ_1 and μ_4 are respectively $\psi(12, \mu_1) = 4.4402326$ and $\psi(12, \mu_4) = 1.2629929$. As we see, the results generated by the angular reconstruction scheme, as described in this paper, are very accurate leading to relative deviations of 0.15 % and 0.35 % respectively for $\psi(12, \mu_1)$ and $\psi(12, \mu_4)$ with respect to the SGF results.

Table III. Angular reconstruction in direction μ_4 ($\mu > 0$) of S_{128} at x = 15 cm and x =20 cm.

Position x (cm)	Angular flux generated by the SGF method μ_4 (8.5463641E-2 [a])	Quadrature set order N	Reconstructed angular flux	δ [b] (%)
15	2.3398091E+00	2	2.332235E+00	0.32371
		4	2.328901E+00	0.46619
		8	2.335839E+00	0.16968
		16	2.338447E+00	0.05821
		32	2.339419E+00	0.01667
		64	2.339730E+00	0.00003
20	3.8153887E-01	2	3.7811633E-01	0.85777
		4	3.7443081E-01	1.86300
		8	3.7709369E-01	1.12571
		16	3.7965879E-01	0.49276
		32	3.8094700E-01	0.15512
		64	3.8140865E-01	0.03413

[a] Read as 8.5463641 x 10^{-2}.
[b] Relative deviation with respect to the angular flux generated by the SGF method.

Table IV. Angular reconstruction in direction μ_{120} ($\mu < 0$) of S_{128} at x = 0 cm and x =10 cm.

Position x (cm)	Angular flux generated by the SGF method μ_{120} (-9.7719849E-01) [a]	Quadrature set order N	Reconstructed angular flux	δ [b] (%)
0	4.3073202E+00	2	4.322609E+00	0.35495
		4	4.285166E+00	0.51448
		8	4.301528E+00	0.13447
		16	4.305899E+00	0.03299
		32	4.306981E+00	0.00787
		64	4.307249E+00	0.00165
10	1.6628689E+00	2	1.585409E+00	4.65821
		4	1.671349E+00	0.50997
		8	1.664285E+00	0.08516
		16	1.663154E+00	0.01715
		32	1.662931E+00	0.00373
		64	1.662881E+00	0.00070

[a] Read as -9.7719849 x 10^{-1}.
[b] Relative deviation with respect to the angular flux generated by the SGF method.

To conclude, Tables III and IV display the angular reconstruction results for the angular fluxes in the directions μ_4 = 0.085463641 and μ_{120} = -0.97719849 of the S_{128} Gauss-Legendre quadrature set at various positions of the slab represented in Fig. 2 using lower-order Gauss-Legendre angular quadrature sets, i.e., S_N, for $N = 2^n$, n = 1 : 6. As a general behavior, we see that the relative deviations decrease as n increases. Therefore, with the present angular reconstruction scheme, it appears that we do not need to run high-order S_N models ("fine-mesh angular discretization"), such as S_{128}, to generate angular fluxes in any angular direction $-1 \le \mu \le 1$,with $\mu \neq 0$.

4. DISCUSSION

We developed earlier the SGF method and showed that it yields numerical solution with no spatial truncation errors regardless of the spatial grid set up on the domain, but apart from computational finite arithmetic considerations [1]. Therefore, one may be able to solve slab-geometry S_N problems with many fewer spatial cells than standard numerical methods, e.g., the linear diamond method [6]. On the other hand, as a drawback of coarse-mesh numerical methods, we note that they do not generate more localized quantities that frequently are needed. Therefore, we have described in this paper two numerical algorithms to reconstruct the coarse-mesh solution within each discretization spatial node, i.e., the spatial reconstruction scheme and the angular reconstruction scheme. According to the numerical results generated for the model problem considered in the previous section by the present reconstruction schemes, we conclude that they are very accurate with respect to the direct calculations. In a sense the numerical algorithms that we offer in this paper constitute inverse problems, since we use converged coarse-mesh results to evaluate more localized solution in the spatial and angular domains. In fact, the reconstruction schemes, as described in this paper, lead to piecewise continuous solution in the spatial and angular ranges where the domain decomposition takes the coarse-mesh discretization nodes as subdomains.

As future work we suggest to implement this concept to energy-dependent S_N problems in slab geometry using the multigroup SGF coarse-mesh results [7]. We plan to report on the multigroup reconstruction schemes after they have been implemented and tested.

ACKNOWLEDGEMENTS

The work by first author (RCB) was supported by Conselho Nacional de Desenvolvimento Científico e Tecnológico (CNPq – Brazil) and Fundação Carlos Chagas Filho de Amparo à Pesquisa do Estado do Rio de Janeiro (FAPERJ – Brazil). The work by the fifth author (DSM), as a graduate student, was supported by Coordenação de Aperfeiçoamento de Pessoal de Nível Superior (CAPES – Brazil).

REFERENCES

1. R.C. Barros and E.W. Larsen, *Nuclear Science and Engineering*, **104**, 199 (1990).

2. R.C. Barros and E.W. Larsen, *Nuclear Science and Engineering*, **111**, 34 (1992).

3. R.C. Barros, H. Alves Filho, E.T. Valero Orellana, F.C. da Silva, N. do Couto, D.S. Dominguez and C.R.G. Hernández, *Progress in Nuclear Energy*, **42**, n^{o}4, 385 (2003).

4. D.S. Dominguez and R.C. Barros, *Annals of Nuclear Energy*, **34**, 958 (2007).

5. J.J. Duderstadt and L.J. Hamilton, *Nuclear Reactor Analysis*, John Wiley & Sons, New York (1976).

6. E.E Lewis and W.F. Miller Jr. *Computational Methods of Neutron Transport*, American Nuclear Society, IL (1993).

7. R.C. Barros and E.W. Larsen, *Transport Theory and Statistical Physics*, **20**, n^{o}586, 441 (1991).